




## Article

# Collision of Bubbles with Solid Surface in the Presence of Specific Surfactants

Maria Zednikova <sup>1,2,\*</sup> , Jakub Crha <sup>1,2</sup> , Lucie Vobecká <sup>2</sup>, Pavlína Basařová <sup>2</sup> , Jiri Vejrazka <sup>1</sup> and Jaroslav Tihon <sup>1</sup>

<sup>1</sup> Institute of Chemical Process Fundamentals of the Czech Academy of Science, v.v.i., 165 02 Prague, Czech Republic; crha@icpf.cas.cz (J.C.); jiri@vejrazka.net (J.V.); tihon@icpf.cas.cz (J.T.)

<sup>2</sup> Department of Chemical Engineering, University of Chemistry and Technology Prague, 166 28 Prague, Czech Republic; lucie.linhartova@vscht.cz (L.V.); pavlina.basarova@vscht.cz (P.B.)

\* Correspondence: zednikova@icpf.cas.cz; Tel.: +420-220-390-251

**Abstract:** The present work is motivated by the effort to understand basic processes occurring in three-phase systems where small bubbles interact with large particles. The simplified system of a single bubble rising in a stagnant liquid and colliding with a solid surface is studied. The effect of two specific surfactants,  $\alpha$ -Terpineol and *n*-Octanol, is investigated. Two independent measurements are combined: (i) bubble–solid surface collision experiments and (ii) the bubble shape oscillations induced by a movable capillary. Both experiments are based on high-speed imaging resulting in the evaluation of the restitution coefficient characterizing the collision process and the relative damping time characterizing the bubble shape oscillations in the presence of surfactants. It was observed that even for small concentrations of a surfactant, both the bubble shape oscillations and the bubble bouncing on the solid surface are significantly suppressed. Two predictions for the restitution coefficient are proposed. The equations include a term characterizing the suppression of the damping time in the presence of surfactants and a term balancing the inertia, capillary and viscous forces in the liquid film separating the bubble and the solid surface. The proposed equations successfully predict the restitution coefficient of bubble bouncing on the solid surface in liquids with the addition of specific surfactants.

**Keywords:** bubble–surface collision; surfactants; bubble oscillations; gas–liquid–solid system; plastics flotation



**Citation:** Zednikova, M.; Crha, J.; Vobecká, L.; Basařová, P.; Vejrazka, J.; Tihon, J. Collision of Bubbles with Solid Surface in the Presence of Specific Surfactants. *Minerals* **2021**, *11*, 442. <https://doi.org/10.3390/min11050442>

Academic Editor: Hyunjung Kim

Received: 25 February 2021

Accepted: 19 April 2021

Published: 21 April 2021

**Publisher's Note:** MDPI stays neutral with regard to jurisdictional claims in published maps and institutional affiliations.



**Copyright:** © 2021 by the authors. Licensee MDPI, Basel, Switzerland. This article is an open access article distributed under the terms and conditions of the Creative Commons Attribution (CC BY) license (<https://creativecommons.org/licenses/by/4.0/>).

## 1. Introduction

Gas–liquid–solid three-phase systems are found in many industrial applications. An important one is the separation of solid materials by flotation. This process is based on the ability of some solids to remain attached to the bubble surface or bubbles to be captured on the solid surface. Particles and bubbles then create agglomerates floating to the liquid surface, from which they can be easily separated [1–4]. The small bubble and larger particle interactions can be simplified by replacing the particle with a horizontal solid surface. The present research is motivated by the study of this simplified system to characterize the effect of surfactants and frothing agents on the interaction process of small bubbles and larger particles.

The process of bubble interaction with a horizontal solid surface was extensively studied both experimentally and theoretically, and various effects were investigated (reviews available in [5,6]). To quantify the process of collision and rebound, the restitution coefficient was used for the case of solid and deformable fluid particles [7–10]. The restitution coefficient  $\varepsilon$  is defined as the ratio of the rebound velocity,  $U_r$ , and the terminal steady rise velocity of the particle,  $U_t$  ( $\varepsilon = U_r/U_t$ ). The coefficient provides an indirect measure of energy dissipation during the particle contact with the solid surface. Its knowledge is

important, e.g., for numerical simulations of complex dispersed systems, where it can be applied to simplify the contact process and hence reduce the computational costs [11].

A scaling of the restitution coefficient based on data for bouncing of solid spheres and liquid drops was reported by Legendre et al. [9] in dependence on the Stokes number of the particle far from the wall. To provide a general scaling, the Stokes number is modified by including an added mass coefficient, which becomes relevant when the fluid particle moves in a liquid with non-negligible inertia [12]. Applying the scaling of the restitution coefficient also for bubble bouncing on a solid surface, the following equations were reported [10]:

$$\varepsilon = \exp \left[ -\frac{\beta_1}{\sqrt{C_m \text{Re}}} \right] \quad (1)$$

$$\varepsilon = \exp \left[ -\beta_2 \sqrt{\frac{\text{Ca}}{C_m \text{Re}}} \right] \quad (2)$$

The Reynolds number ( $\text{Re} = \rho D_b U_t / \mu$ ) provides the comparison of the bubble inertia relative to the viscous forces induced by the film drainage between the bubble and the solid surface. The capillary number ( $\text{Ca} = U_t \cdot \mu / \sigma$ ) then gives the ratio of bubble inertia relative to the bubble surface force. Here,  $\rho$  and  $\mu$  are the density and viscosity of the liquid, respectively,  $D_b$  is the equivalent bubble diameter, and  $\sigma$  stands for the surface tension. The added mass coefficient  $C_m$  is assumed far from the solid surface and generally, its value depends on the actual bubble aspect ratio. For spherical bubbles, it attains the value  $C_m = 0.5$  (far from the wall) and  $C_m = 0.73$  (touching the wall) [8,12–14]. For oblate bubbles, it can be calculated from the kinetic energy of the potential flow around an ellipsoidal bubble approaching the wall [14,15].

Note, the term  $C_m \text{Re}$  is proportional to the modified Stokes number  $\text{St}^*$  defined in the works of Legendre [8–10]. Assuming that the density of the dispersed phase (air) is negligible to the density of the continuous phase (water), the relation  $C_m \text{Re} = 9\text{St}^*$  holds. The values of the parameters  $\beta_1$  and  $\beta_2$  (10.5 and 90, respectively) were obtained by fitting the experimental data [8–10] (see also in [16]).

Equations (1) and (2) provide the restitution coefficient of bubbles bouncing in pure liquids, however, the values of the parameters  $\beta_1$  and  $\beta_2$  vary in the presence of surfactants [16]. The effect of surfactants on the bubble bouncing process has been intensively studied by the group of Malysa [17–21]. The presence of surfactants significantly suppresses the bubble velocity, shape deformations, and rebound from the surface. This suggests that the energy is dissipated not only by viscous stresses in the thin liquid film but also by other stresses associated with the adsorption/desorption of the surfactant on the bubble interface. However, no quantification of the surfactant concentration effect on the restitution coefficient has been published yet.

Bubble dynamics and bubble shape deformations are very sensitive even to low interface contaminations or low concentrations of surface-active agents [22–25]. The bubble interface behavior is primarily linked to the instantaneous variations of the surface tension induced by interfacial area changes, i.e., to the dilatational rheology of the interfacial layer. The parameters quantifying the interface rheology are the dilatational surface elasticity and viscosity. In the case of non-micellar solutions, the dilatational surface elasticity characterizes the recoverable energy stored in the surface and the dilatational surface viscosity reflects the energy dissipation through the surface relaxation processes [26]. The commercial measurements of interface rheology are based on the oscillating drop/bubble methods [27,28]. Assuming the model of diffusion-controlled relaxation processes, the surface dilatational rheology has been evaluated quantitatively [29]. From the drop/bubble oscillation experiments, another parameter related to the drop/bubble interface rheology can be evaluated—the damping time or damping rate of bubble shape oscillations. As well as the dilatational surface viscosity, the damping rate is also a measure of energy dissipation during the interface variations, thus both variables are interlinked. When no damping is observed, the interface is purely elastic, i.e., the surfactant exchange between the interface

and the bulk is negligible and the elasticity modulus is determined by the equilibrium between the surface pressure and the surfactant surface concentration [30]. When the damping of surface oscillation occurs, the surface energy is dissipated at the interface. In the case of non-micellar soluble surfactants, the surface energy dissipation is related to the surfactant exchange between the interface and the bulk during the relaxation processes. Other relaxation processes relevant for other types of surfactants can be (i) exchange of the surfactant between micelles and the bulk solution, (ii) slow adsorption/desorption because of barriers at the surface, and (iii) in-surface reactions [30]. These processes may occur when micellar surfactants or macromolecules (e.g., proteins, polymers) exist in the solution.

The damping time/rate can be also used as a suitable quantity to assess the effect of surfactant presence on the bubble interface properties [22,31–33]. Regarding our previous experience in the quantification of restitution coefficients [16] and damping rates of bubble shape oscillations [34], we aim to couple the results of these two independent experiments. To characterize the effect of surfactants on the restitution coefficient, two measurements were performed and analyzed: (i) bubble–solid surface bouncing experiment resulting in restitution coefficient values and (ii) bubble shape oscillation experiments resulting in values of the damping time for various surfactant concentrations.

The work is limited by two specific surfactants:  $\alpha$ -Terpineol and *n*-Octanol, which are nonionic non-micellar surfactants often used as frothing agents [35,36].  $\alpha$ -Terpineol is a popular fragrance ingredient used in perfumes, cosmetics, and household cleaning products. In addition, the important biological properties of  $\alpha$ -Terpineol increase its interest also in medicine and the pharmaceutical industry [37,38]. *n*-Octanol is a surface-active agent often used as a model surfactant partially soluble in water and with known surface-active properties [39]. Another surface-active property of *n*-Octanol arises from the enhancement of the foamability in combination with other ionic surfactants [40,41]. These two surfactants were used in several articles dealing with the bubble dynamics and bubble–solid surface interactions [18,21,42]. However, the quantification of their effect on the restitution coefficient has not been provided yet. Therefore, this work aims to provide new predictions of the restitution coefficient, which will also include the effects caused by the presence of these two surfactants.

## 2. Materials and Methods

### 2.1. Experimental Setup and Used Materials

The experimental setup used for both types of experiments is illustrated in Figure 1. The setup consists of a rectangular cell of 110 mm  $\times$  110 mm  $\times$  260 mm in size (2 L working volume), a device with a moveable capillary [43], a light source and the high-speed camera Photron Fastcam SA1.1 (Photron Ltd., Tokyo, Japan). The device with movable capillary [43] enables to produce a bubble with a defined size for collision experiments and an oscillating bubble for oscillation experiments. A capillary of inner diameter 250  $\mu$ m is used to form bubbles with sizes ranging from 0.4 to 1.9 mm.

The experiments were performed for deionized water and for aqueous solutions of  $\alpha$ -Terpineol and *n*-Octanol of the same concentrations ( $0.1 \times 10^{-3}$ ,  $0.3 \times 10^{-3}$  and  $1.0 \times 10^{-3}$  mol/L). The results of our new experiments were combined with data published in our previous works [16,34]. Deionized water with a final conductivity of 1.1  $\mu$ S/cm was obtained by distillation and additional filtration through activated carbon and ion-exchange resin. The density, viscosity, and surface tension were measured to characterize the physical-chemical properties of all used liquids. The static surface tension was measured with the tensiometer Krüss K11 (KRÜSS GmbH, Hamburg, Germany) using the du Noüy ring method. The dynamic surface tension (dependence of surface tension on the bubble surface age) was measured by the tensiometer Krüss BP 100 (KRÜSS GmbH, Hamburg, Germany). The values of dynamic surface tension relevant to the first bubble–wall collision were obtained for aging times between 2 and 5 s (depending on the bubble size and the corresponding rise velocity). The viscosity is measured by the Ubbelohde viscosimeter (Type U 0, constant 0.001, TECHNICKÉ SKLO, n. p., Držkov, Czech Republic) and the

density by balancing the immersed solid body of known volume (Krüss K11). During the measurements of liquid properties and subsequent experiments, the temperature was maintained at 20 °C. The addition of surfactants does not change the values of density and viscosity, even for the most concentrated solutions. The physical-chemical properties of all investigated liquids are given in Table 1. The glass plate provided a horizontal surface for the bubble collision experiments. The plate was cleaned by chromosulfuric acid to ensure the hydrophilicity of the surface and to avoid the effect of surface roughness on the collision process [18]. The zeta-potential and the pH were not measured in the present experiments, because no effects of non-ionic surfactants on both the bubble surface charge [44,45] and the charge of quartz surfaces similar to glass [46,47] were found.

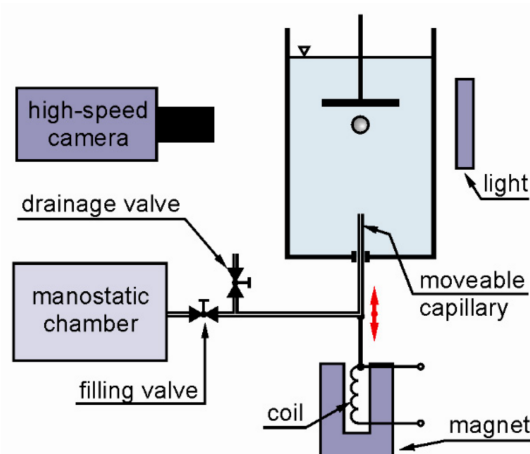


Figure 1. Experimental setup.

**Table 1.** Physical-chemical properties of all used liquids. The dynamic surface tension corresponds to the moment of the first contact of the bubble with the solid surface. The bubble aging time corresponding to this moment varies in dependence on the bubble size and the corresponding velocity.

Liquid	Density (kg/m <sup>3</sup> )	Viscosity (mPa·s)	Surface Tension (Static) (mN/m)	Surface Tension (Dynamic) (mN/m)
Deionized water <sup>1</sup>	998	1.002	72.2	72.2
$\alpha$ -Terpineol $0.1 \times 10^{-3}$ mol/L <sup>1</sup>	998	1.000	71.6	71.8
$\alpha$ -Terpineol $0.3 \times 10^{-3}$ mol/L <sup>1</sup>	998	1.000	70.1	71.0
$\alpha$ -Terpineol $1.0 \times 10^{-3}$ mol/L <sup>1</sup>	998	1.000	64.3	67.5
<i>n</i> -Octanol $0.1 \times 10^{-3}$ mol/L	998	1.000	71.0	71.0
<i>n</i> -Octanol $0.3 \times 10^{-3}$ mol/L	998	1.000	67.8	69.0
<i>n</i> -Octanol $1.0 \times 10^{-3}$ mol/L	998	1.000	55.2	59.5

<sup>1</sup> Physical-chemical properties correspond to the data in [16].

The surface tension for solutions of both surfactants was measured in a wide range of concentrations to provide sufficient data for the evaluation of adsorption isotherms (Figure 2). Using the Gibbs adsorption equation and the non-linear Langmuir shape of the isotherm, the constants  $\Gamma_m$  and  $K_L$  were obtained by fitting the experimental data ( $\Gamma_m = 4.61 \times 10^{-6}$  mol/m<sup>2</sup>,  $K_L = 1.36$  m<sup>3</sup>/mol for  $\alpha$ -Terpineol solutions;  $\Gamma_m = 9.44 \times 10^{-6}$  mol/m<sup>2</sup>,  $K_L = 1.30$  m<sup>3</sup>/mol for *n*-Octanol solutions). The constant  $\Gamma_m$  represents the theoretical maximum surfactant concentration at the interface and the constant  $K_L$  is the Langmuir equilibrium adsorption constant providing a useful measure of the surface activity of the surfactant [48].

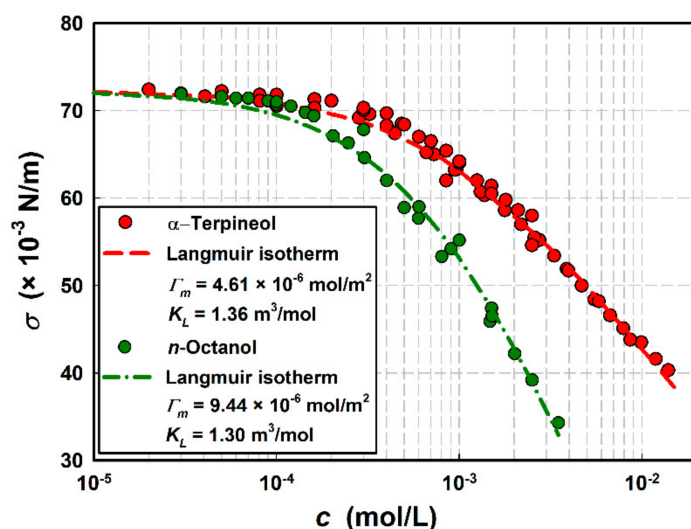


Figure 2. Surface tension in dependence on the concentration of surfactant. Evolution of Langmuir isotherm for solutions of both surfactants.

2.2. Bubble Collision Experiment

The bubble–wall collision experiment consists of bubble generation, bubble free rise, and bubble bouncing on the horizontal solid surface. The whole process is recorded by the high-speed camera Photron Fastcam SA1.1 (Photron Ltd., Tokyo, Japan) with a macroscopic lens (5400 fps, 1024 pix × 1024 pix, 10 μm/pix). The sequence of images is treated to obtain the bubble position and the boundary using the procedure described previously [16]. With the assumption of axial symmetry of the bubble, the center-of-mass position, volume, and surface area of the bubble are evaluated for each image. The equivalent bubble size  $D_b$  is determined from the images captured long before the bubble–wall collision as the diameter of a sphere with the same volume. The instantaneous bubble velocity is obtained by differentiating the center-of-mass positions of the bubble obtained from a time sequence of images. An example of the time evolution of the bubble’s center-of-mass position (left y-axis) and velocity (right axis) is shown in Figure 3 (negative sign of  $y/R_b$  indicates the bubble under the wall). The bubble terminal velocity  $U_t$  is the steady state value of the rise velocity achieved before it starts to feel the presence of a solid surface. It is determined by velocity averaging over a proper period of time.

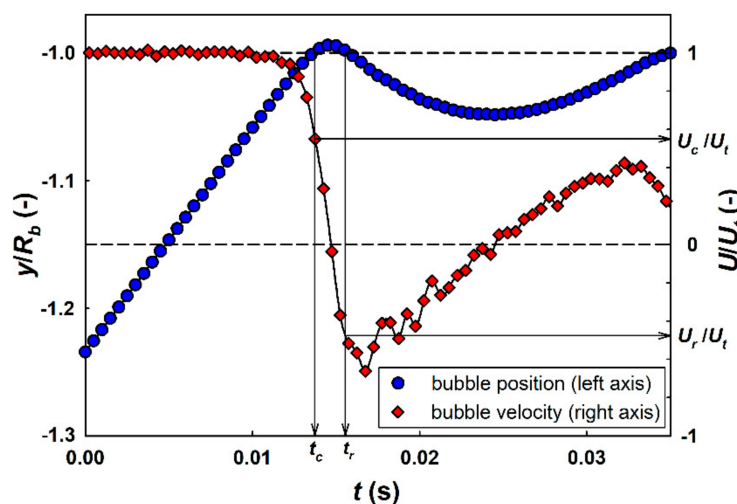


Figure 3. Time dependence of normalized bubble position (left y-axis) and velocity (right y-axis). Explanation of impact and rebound moment evaluation. Deionized water,  $D_b = 1.05$  mm.

Figure 3 also demonstrates the determination of the instants of the bubble impact  $t_c$  and the rebound  $t_r$ . They are defined as the moments when the distance between the center-of-mass of the bubble and the solid surface is equal to the equivalent bubble radius  $R_b$ . In Figure 3, both moments are represented by the points where the normalized bubble position (blue circles) crosses the horizontal line with the ordinate  $-1.0$ . Note that the impact and rebound instants cannot be defined exactly, as the bubble and the wall are always separated by a liquid film (and hence no real contact exists) until the rupture of the liquid film and the three-phase-contact line formation. The impact and rebound velocities,  $U_c$  and  $U_r$ , are defined as the velocities corresponding to the impact and rebound moments (see indication by arrows in Figure 3). The present definition of both instants is equivalent to the definition provided by Legendre et al. [8]. The different definitions of these instants would lead to slightly different values of impact and rebound velocities. In the present work, only the first rebound of the bubble from the surface is analyzed.

### 2.3. Bubble Shape Oscillation Experiment

The experiments of bubble shape oscillations are performed by the same procedure as published in our previous works [22,34]. The experiment starts by the bubble growth at the capillary. After reaching a suitable bubble size (typically around 1.2 mm), the capillary suddenly moves upwards and induces bubble shape oscillations. The needle movement is controlled to keep the bubble attached to the capillary. The whole process is recorded by the high-speed camera Photron Fastcam SA1.1 (Photron Ltd., Tokyo, Japan) with a macroscopic lens (10,000 fps, 700 pix  $\times$  384 pix, 5  $\mu\text{m}/\text{pix}$ ).

The image processing of each image provides the experimental bubble boundary, which is fitted by a function to obtain the coefficients necessary to evaluate the damping time of the shape oscillations. The fitting function assumes the axial symmetry of the bubble and harmonic oscillations around a spherical bubble of diameter  $D_b$ . The function is decomposed into Legendre polynomials with the coefficients  $a_i$  characterizing the actual bubble shape [49]. The degree of the Legendre polynomial (index  $i$ ) characterizes the differences from the given spherical shape (oscillation modes):  $a_0$  (mode 0) describes the volume changes,  $a_1$  (mode 1) describes the bubble displacement,  $a_2$  (mode 2) describes the limiting cases of the ellipsoid-like shape,  $a_3$  (mode 3) describes the deformation in a shape with three lobes, etc. For a detailed description, see Vejrazka et al. [34] (their Figure 2). The processing of the whole image sequence provides the time evolution of coefficients  $a_i$  following the cosine functions (Figure 4a) with decreasing amplitudes  $A_i$ .

The amplitudes decrease exponentially with the damping time  $\tau_i$  as an exponent parameter (Figure 4b), which is evaluated by fitting the time dependence curve of the amplitudes  $A_i$  by Equation (3)

$$A_i = c_i \exp\left(-\frac{t}{\tau_i}\right) \quad i = 2, \dots, 8 \quad (3)$$

where  $c_i$  and  $\tau_i$  are the fitted parameters. Figure 4b shows the time dependence of the amplitudes  $A_i$  for three oscillation modes (2, 3, and 4) in a semi-logarithmic representation. The amplitudes are evaluated in three ways: (i) peak-to-peak (p2p) evaluation corresponds to the difference between the two adjacent maximum and the minimum divided by 2; (ii) maximum values of the amplitude (max); (iii) absolute values of the minimum amplitude (min). As the slopes of the lines for the presented modes are practically the same (see Figure 4b), the damping time is evaluated from the slope for mode 2 only because this value was proved to be the most reliable [34].

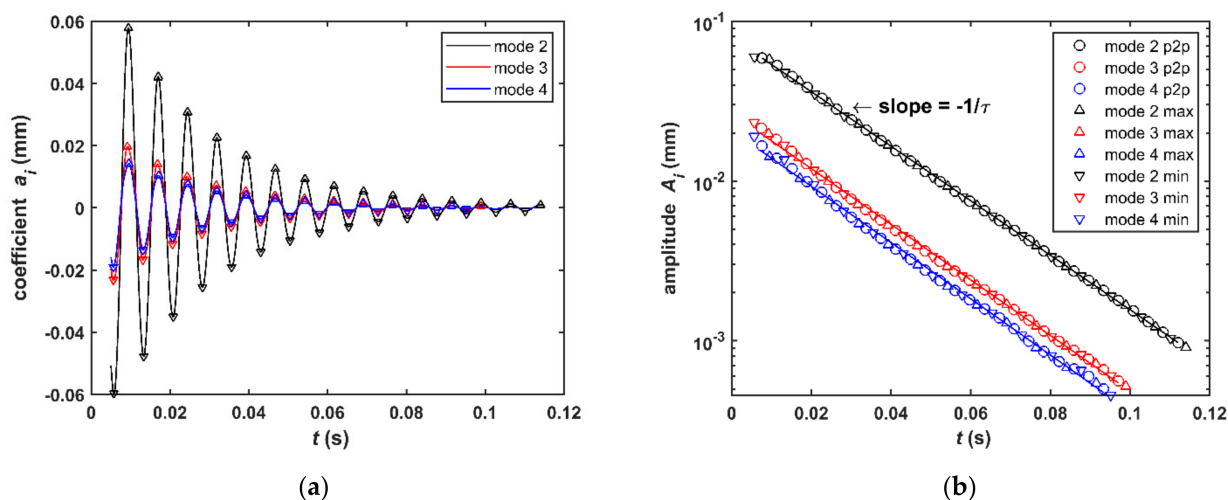


**Figure 4.** The evaluation of bubble shape oscillations for  $0.1 \times 10^{-3}$  mol/L *n*-Octanol solution, bubble size  $D_b = 1.173$  mm, time  $t = 0$  s corresponds to the end of the needle movement; (a) time dependence of Legendre polynomial coefficient  $a_i$  for mode 2, 3 and 4; (b) time dependence of amplitudes  $A_i$  for modes 2, 3 and 4.

### 3. Results and Discussion

#### 3.1. Restitution Coefficient

As it was observed in our previous study [16], the presence of  $\alpha$ -Terpineol suppresses the bubble rebound from the solid surface. This suppression can be quantified by decreasing the restitution coefficient  $\varepsilon$  (Figure 5a,b), where  $\varepsilon = 0$  denotes a zero-value of the bubble rebound velocity and hence no rebound from the solid surface. The restitution coefficient represents the energy dissipation during the drainage of the liquid film when the bubble approaches the solid surface. According to the scaling proposed by Legendre et al. [8–10], the restitution coefficient can be expressed as an exponential function of the inverse value of the modified Reynolds number (Equation (1)) or as a function of the ratio of the capillary number and the modified Reynolds number (Equation (2)). Both equations cover the effect of bubble size and liquid inertia but do not cover the presence of surfactants (Figure 5). Even Equation (2), which also considers the capillary forces at the bubble interface by including the capillary number, does not reflect the changes in the restitution coefficient (Figure 5b) when surface-active agents are present in the liquid. Comparing both surfactants, the decrease of restitution coefficient is more significant in the solutions of *n*-Octanol. For example, similar values of restitution coefficients were obtained for the lowest concentration ( $0.1 \times 10^{-3}$  mol/L) of the *n*-Octanol solution and for the middle concentration ( $0.3 \times 10^{-3}$  mol/L) of the  $\alpha$ -Terpineol solution. When the surface tension under static conditions (Table 1) or the evolution of Langmuir isotherms (Figure 2) are compared, it can be found that both these solutions slightly differ in the magnitude of surface tension. Even the dynamic surface tension is not a suitable correlation parameter, although its magnitude obtained for the two surfactant solutions with similar restitution coefficients is the same. The small decrease in dynamic surface tension, which only slightly exceeds the expected experimental error ( $\pm 0.5$  mN/m), cannot explain the significant changes in the restitution coefficient. A more significant decrease of the surface tension was only found for the high concentrated solutions where no bubble rebound from the surface is observed. Thus, neither the static nor the dynamic surface tension would help characterize the decrease of the restitution coefficient in the presence of surfactants.

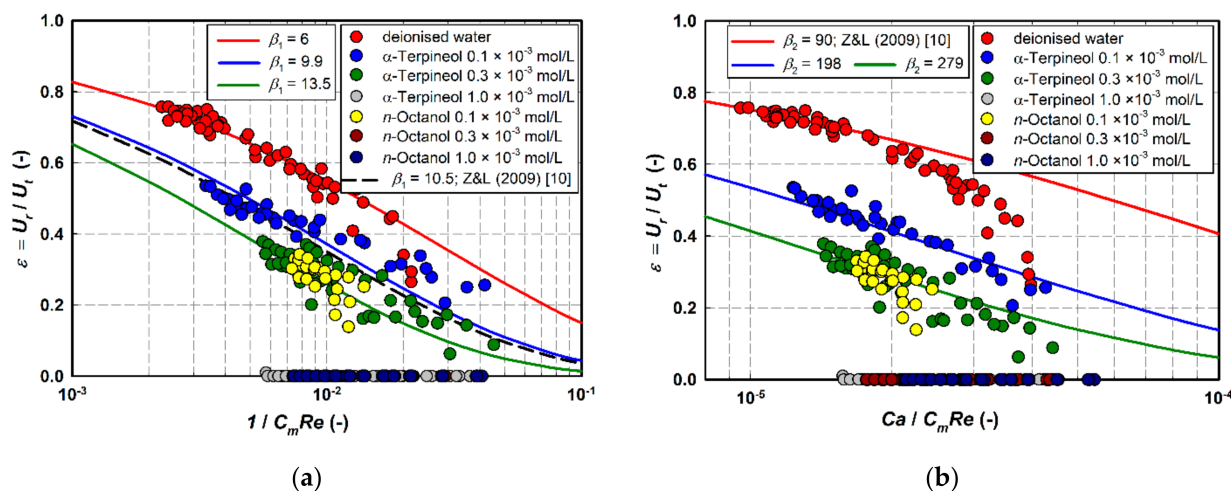


**Figure 5.** The restitution coefficient for the used liquids; (a) expression of Equation (1), where the restitution coefficient is the exponential function of the inverse value of the square root of the modified Reynolds number; (b) expression of Equation (2), where the restitution coefficient is the exponential function of the square root ratio of the capillary number and the modified Reynolds number.

To analyze the results, a detailed description of the bouncing process is needed. The bubble approaching the solid surface starts to decelerate and deform from its original shape due to the increase of pressure in a liquid film separating the bubble and the solid surface. The lubrication force in a liquid film, which is opposing the bubble inertia and the bubble surface force, becomes significant. A part of the bubble kinetic energy is dissipated in the film due to viscosity effects and another part is stored in the bubble deformation resulting in the increase of the bubble interface.

In the case of large deformations and small viscous dissipations (e.g., bubbles in distilled water), the kinetic energy recovers and the bubble rebounds from the surface. The rebound of bubbles from the solid surface is then controlled by three forces: the inertial force, the lubrication force due to viscous dissipation in the film, and the surface force. The term  $Ca / (C_m Re)$  includes all these forces and is sufficient to describe the restitution coefficient for pure liquids.

The presence of surface-active agents causes additional energy dissipation at the bubble interface [16]. The possible mechanism of the additional energy loss can be associated with the surface viscosity of the interface covered by surfactants and/or with the Marangoni stresses caused by the uneven distribution of the surfactant molecules at the bubble interface. No matter which mechanism is relevant, the formation of a new interface due to the bubble shape deformation during the collision process induces the adsorption/desorption of surfactants leading to an additional energy loss. To provide the proper scaling of the restitution coefficient in the presence of surfactants, an independent study of bubble shape oscillations was performed.

### 3.2. Damping Time of Bubble Shape Oscillations

The damping time was measured for a wide range of surfactant concentrations, including those used in bubble collision experiments. To eliminate the effect of the bubble size, the absolute value of the damping time  $\tau$  ( $\sim 10^1$  ms) is normalized by the characteristic viscous time ( $\sim 10^3$  ms)

$$\tau_d = \frac{\tau}{\rho D_b^2 / \mu} \quad (4)$$

where  $\rho$  and  $\mu$  are the liquid density and viscosity, respectively. The characteristic viscous time expresses the scale of the damping time due to normal viscous dissipation in the liquid moving around the oscillating bubble [15,49].



The observed decrease in the dimensionless damping time with increasing surfactant concentration is shown in Figure 6. To better characterize the effect of surfactants, the dimensionless damping times measured in surfactant solutions are related to those measured in distilled water (subscript  $w$  refers to pure water). For comparison, the relative values of the surface tension are also shown in Figure 6. From both the damping time and surface tension curves, it is evident that the addition of  $n$ -Octanol (green symbols) causes more significant changes in surface activity and faster damping of the bubble shape oscillations than the same addition of  $\alpha$ -Terpineol (red symbols). The obtained faster damping also suggests more significant energy dissipation at the bubble interface [26,28] and hence higher surface viscosity of the  $n$ -Octanol monolayer than that of the  $\alpha$ -Terpineol monolayer. Moreover, the damping times for the  $n$ -Octanol solutions with concentrations higher than  $0.5 \times 10^{-3}$  mol/L are so small (and the bubble oscillations dampen so fast) that their values are not measurable by the present technique.

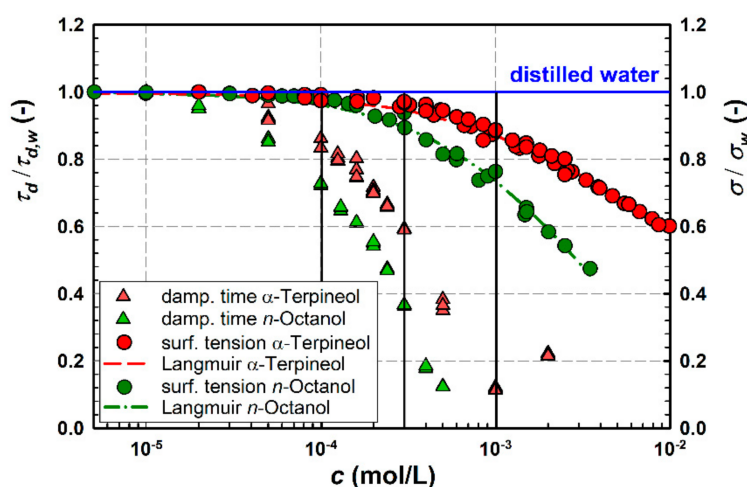


**Figure 6.** Relative decrease of the dimensionless damping time (triangles, left axis) and the relative decrease of surface tension (circles, right axis) in dependence on the surfactant concentration. The blue solid line represents the distilled water; black solid lines indicate the concentrations used for collision experiments.

Figure 6 also presents the differences in the relative decrease of the damping time and in the relative decrease of the surface tension. If the results obtained for the smallest concentration of surfactants used in our experiments are compared (see values on the black solid line corresponding to  $c = 10^{-4}$  mol/L), the relative decrease of the surface tension is negligible for both surfactants, whereas the decrease in the damping time observed for the  $n$ -Octanol solution ( $\tau_d/\tau_{d,w} = 0.726$ ) is much more significant than that for the  $\alpha$ -Terpineol solution ( $\tau_d/\tau_{d,w} = 0.840$ ).

In the next section, the experimental values obtained for relative damping times are used to better correlate the results of the restitution coefficients.

### 3.3. Correlation of Restitution Coefficient with the Relative Damping Time

As it was mentioned in Section 3.1., the study of bubble shape oscillations and their damping can be helpful to characterize the bubble–solid surface collision when surfactants are present in the liquid. Both scaling Equations (1) and (2) can be extended by including the relative damping time  $\tau_d/\tau_{d,s}$ , and thus are rewritten in the following forms

$$\varepsilon = \exp \left[ -\gamma_1 \left( \frac{\tau_d}{\tau_{d,s}} \right)^{\delta_1} \frac{1}{\sqrt{C_m \text{Re}}} \right] \quad (5)$$

$$\varepsilon = \exp \left[ -\gamma_2 \left( \frac{\tau_d}{\tau_{d,s}} \right)^{\delta_2} \sqrt{\frac{Ca}{C_m Re}} \right] \tag{6}$$

Here, the index *s* stands for a solvent in general and the parameters  $\gamma_1, \delta_1$  and  $\gamma_2, \delta_2$  are obtained by fitting the experimental data (for their particular values see Table 2). Figure 7 compares the final fits of Equations (5) and (6) to the measured values of the restitution coefficients. Although, the close-fitting of the equations is not perfect, after including the term of the relative damping time into the scaling, the effect of surfactants on the decrease of the restitution coefficient is satisfactorily described for the studied  $\alpha$ -Terpineol and *n*-Octanol. The values of restitution coefficient obtained in the  $1 \times 10^{-3}$  mol/L *n*-Octanol solution were excluded from the fitting, as the corresponding damping time was unmeasurable by the present technique.

**Table 2.** Optimized parameters of Equations (5) and (6) for the prediction of the restitution coefficient.

Equation	$\gamma_i$ (-)	$\delta_i$ (-)	$R^2$ (-)
(5)	6.9	-1.40	0.96
(6)	123	-1.87	0.95

$\gamma_i$  represents the particular parameters  $\gamma_1$  and  $\gamma_2$ ;  $\delta_i$  represents the particular parameters  $\delta_1$  and  $\delta_2$ ;  $R^2$  is the coefficients of determination.

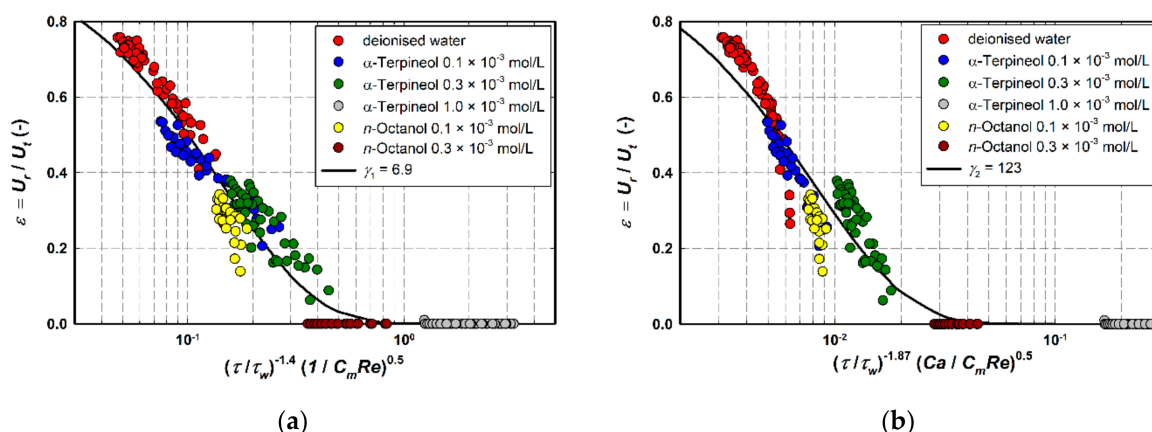


**Figure 7.** Prediction of the restitution coefficient for the used liquids; (a) expression for Equation (5); (b) expression for Equation (6).

Comparing both types of scaling, Equation (5) seems to be more appropriate for data fitting (compare the coefficients of determination  $R^2$ ). It can be caused by the fact that the surface tension forces, which characterize the ability of the interface to be deformed, are included into Equation (6) twice: first in the form of the capillary number and then also in the form of the relative damping time. However still, both types of equations predict successfully the restitution coefficients of the bubble–solid surface collision in water solutions of two specific types of surfactants.

#### 4. Conclusions

The process of bubble bouncing on a hydrophilic solid surface in a liquid is studied experimentally. The restitution coefficients characterizing the energy dissipation during the bubble contact with the solid surface are obtained for different bubble sizes and concentrations for two specific types of surfactants,  $\alpha$ -Terpineol and *n*-Octanol.

The presence of surface-active agents in water affects the bubble dynamics, shape deformations, and hence the restitution coefficient. Even for a small concentration of surfactant, which has no effect on its physical properties, both the bubble shape oscillations and the bubble bouncing on the solid surface are significantly suppressed. The surfactant

adsorption/desorption from the bubble interface plays a significant role in the bouncing process and hence needs to be included into the prediction equation of the restitution coefficient. New forms of these equations are suggested. The original equations based on the scaling proposed by Zenit and Legendre [9,10] are extended by a term characterizing the effect of surfactants on the bubble shape oscillations. The term is the relative damping time of the bubble shape oscillations, which is defined as the ratio of damping time obtained in the surfactant solution and in pure solvent (water in the present case). This relative damping time is obtained by an independent experimental technique based on the study of bubble shape oscillations induced by a movable capillary. The proposed Equations (5) and (6) successfully predict the restitution coefficient of bubble bouncing on the solid surface in liquids with the addition of surfactants. The parameters of these equations (given in Table 2) are optimized and thus also limited to the two specific surfactants ( $\alpha$ -Terpineol and *n*-Octanol) and their validity for other types of surfactants should be proved.

**Author Contributions:** Conceptualization, M.Z. and J.V.; writing—original draft preparation, M.Z.; design of experiments, routine measurements, L.V. and J.C.; software, M.Z., J.V. and J.C.; data analysis and interpretation, M.Z., J.V., P.B. and J.T.; writing—review and editing, P.B. and J.T.; funding acquisition, P.B. All authors have read and agreed to the published version of the manuscript.

**Funding:** This research was funded by The Czech Science Foundation (GACR), grant number 19-09518S.

**Institutional Review Board Statement:** Not Applicable.

**Informed Consent Statement:** Not Applicable.

**Data Availability Statement:** Not Applicable.

**Conflicts of Interest:** The authors declare no conflict of interest.

## References

1. Dai, Z.F.; Fornasiero, D.; Ralston, J. Particle-bubble collision models—A review. *Adv. Colloid Interface Sci.* **2000**, *85*, 231–256. [[CrossRef](#)]
2. Nguyen, A.V.; Schulze, H.J. *Colloidal Science of Flotation*; Marcel Dekker: New York, NY, USA; Basel, Switzerland, 2004.
3. Hubicka, M.; Basarova, P.; Vejrazka, J. Collision of a small rising bubble with a large falling particle. *Int. J. Miner. Process.* **2013**, *121*, 21–30. [[CrossRef](#)]
4. Basarova, P.; Zawala, J.; Zednikova, M. Interactions between a Small Bubble and a Greater Solid Particle during the Flotation Process. *Miner. Process Extr. Metall. Rev.* **2019**, *40*, 410–426. [[CrossRef](#)]
5. Emery, T.S.; Kandlikar, S.G. Film Size during Bubble Collision with a Solid Surface. *J. Fluids Eng.* **2019**, *141*. [[CrossRef](#)]
6. Manica, R.; Klaseboer, E.; Chan, D.Y.C. The hydrodynamics of bubble rise and impact with solid surfaces. *Adv. Colloid Interface Sci.* **2016**, *235*, 214–232. [[CrossRef](#)] [[PubMed](#)]
7. Joseph, G.G.; Zenit, R.; Hunt, M.L.; Rosenwinkel, A.M. Particle-wall collisions in a viscous fluid. *J. Fluid Mech.* **2001**, *433*, 329–346. [[CrossRef](#)]
8. Legendre, D.; Daniel, C.; Guiraud, P. Experimental study of a drop bouncing on a wall in a liquid. *Phys. Fluids* **2005**, *17*, 097105. [[CrossRef](#)]
9. Legendre, D.; Zenit, R.; Daniel, C.; Guiraud, P. A note on the modelling of the bouncing of spherical drops or solid spheres on a wall in viscous fluid. *Chem. Eng. Sci.* **2006**, *61*, 3543–3549. [[CrossRef](#)]
10. Zenit, R.; Legendre, D. The coefficient of restitution for air bubbles colliding against solid walls in viscous liquids. *Phys. Fluids* **2009**, *21*, 083306. [[CrossRef](#)]
11. Hadinoto, K.; Curtis, J.S. Effect of interstitial fluid on particle-particle interactions in kinetic theory approach of dilute turbulent fluid-particle flow. *Ind. Eng. Chem. Res.* **2004**, *43*, 3604–3615. [[CrossRef](#)]
12. Magnaudet, J.; Eames, I. The motion of high-Reynolds-number bubbles in inhomogeneous flows. *Ann. Rev. Fluid Mech.* **2000**, *32*, 659–708. [[CrossRef](#)]
13. Milne-Thomson, L.M. *Theoretical Hydrodynamics*, Dover ed.; Dover Publications: New York, NY, USA, 1996.
14. Simcik, M.; Ruzicka, M.C.; Drahos, J. Computing the added mass of dispersed particles. *Chem. Eng. Sci.* **2008**, *63*, 4580–4595. [[CrossRef](#)]
15. Lamb, H. *Hydrodynamics*, 6th ed.; Cambridge University Press: London, UK, 1975.
16. Fujasova-Zednikova, M.; Vobecka, L.; Vejrazka, J. Effect of solid material and surfactant presence on interactions of bubbles with horizontal solid surface. *Can. J. Chem. Eng.* **2010**, *88*, 473–481. [[CrossRef](#)]

17. Malysa, K.; Krasowska, M.; Krzan, M. Influence of surface active substances on bubble motion and collision with various interfaces. *Adv. Colloid Interface Sci.* **2005**, *114*, 205–225. [[CrossRef](#)]
18. Kosior, D.; Zawala, J.; Krasowska, M.; Malysa, K. Influence of n-octanol and alpha-terpineol on thin film stability and bubble attachment to hydrophobic surface. *Phys. Chem. Chem. Phys.* **2013**, *15*, 2586–2595. [[CrossRef](#)]
19. Kosior, D.; Zawala, J.; Malysa, K. Influence of n-octanol on the bubble impact velocity, bouncing and the three phase contact formation at hydrophobic solid surfaces. *Colloid Surf. A-Physicochem. Eng. Asp.* **2014**, *441*, 788–795. [[CrossRef](#)]
20. Kosior, D.; Zawala, J.; Niecikowska, A.; Malysa, K. Influence of non-ionic and ionic surfactants on kinetics of the bubble attachment to hydrophilic and hydrophobic solids. *Colloid Surf. A-Physicochem. Eng. Asp.* **2015**, *470*, 333–341. [[CrossRef](#)]
21. Zawala, J.; Kosior, D.; Dabros, T.; Malysa, K. Influence of bubble surface fluidity on collision kinetics and attachment to hydrophobic solids. *Colloid Surf. A-Physicochem. Eng. Asp.* **2016**, *505*, 47–55. [[CrossRef](#)]
22. Abi Chebel, N.A.; Vejrazka, J.; Masbernat, O.; Risso, F. Shape oscillations of an oil drop rising in water: Effect of surface contamination. *J. Fluid Mech.* **2012**, *702*, 533–542. [[CrossRef](#)]
23. Orvalho, S.; Stikova, L.; Stanovsky, P.; Zednikova, M.; Vejrazka, J.; Ruzicka, M. Influence of bubble approach velocity on coalescence in alpha-terpineol and n-octanol solutions. *Physicochem. Probl. Mineral Pro.* **2018**, *54*, 73–80.
24. Basarova, P.; Pislova, J.; Mills, J.; Orvalho, S. Influence of molecular structure of alcohol-water mixtures on bubble behaviour and bubble surface mobility. *Chem. Eng. Sci.* **2018**, *192*, 74–84. [[CrossRef](#)]
25. Basarova, P.; Kryvel, Y.; Crha, J. Bubble Rise Velocity and Surface Mobility in Aqueous Solutions of Sodium Dodecyl Sulphate and n-Propanol. *Minerals* **2019**, *9*, 743. [[CrossRef](#)]
26. Miller, R.; Liggieri, L. *Interfacial Rheology*; Brill: Leiden, The Netherlands; Boston, MA, USA, 2009.
27. Ravera, E.; Liggieri, L.; Loglio, G. Dilational rheology of adsorbed layers by oscillating drops and bubbles. In *Interfacial Rheology*; Miller, R., Liggieri, L., Eds.; Brill: Leiden, The Netherlands; Boston, MA, USA, 2009; pp. 137–177.
28. Langevin, D. Rheology of Adsorbed Surfactant Monolayers at Fluid Surfaces. *Ann. Rev. Fluid Mech.* **2014**, *46*, 47–65. [[CrossRef](#)]
29. Lucassen, J.; van den Tempel, M. Dynamic Measurements of Dilational Properties of a Liquid Interface. *Chem. Eng. Sci.* **1972**, *27*, 1283–1291. [[CrossRef](#)]
30. Lucassen-Reynders, E.H.; Lucassen, J. Surface dilational rheology: Past and present. In *Interfacial Rheology*; Miller, R., Liggieri, L., Eds.; Brill: Leiden, The Netherlands; Boston, MA, USA, 2009.
31. Asaki, T.J.; Marston, P.L. Free Decay of Shape Oscillations of Bubbles Acoustically Trapped in Water and Sea-Water. *J. Fluid Mech.* **1995**, *300*, 149–167. [[CrossRef](#)]
32. Asaki, T.J.; Marston, P.L. The effects of a soluble surfactant on quadrupole shape oscillations and dissolution of air bubbles in water. *J. Acoust. Soc. Am.* **1997**, *102*, 3372–3377. [[CrossRef](#)]
33. Asaki, T.J.; Thiessen, D.B.; Marston, P.L. Effect of an Insoluble Surfactant on Capillary Oscillations of Bubbles in Water—Observation of a Maximum in the Damping. *Phys. Rev. Lett.* **1995**, *75*, 2686–2689. [[CrossRef](#)]
34. Vejrazka, J.; Vobecka, L.; Orvalho, S.; Zednikova, M.; Tihon, J. Shape oscillations of a bubble or drop attached to a capillary tip. *Chem. Eng. Sci.* **2014**, *116*, 359–371. [[CrossRef](#)]
35. Laskowski, J.S.; Woodburn, E.T. *Frothing in Flotation II: Recent Advances in Coal Processing*; CRC Press: Boca Raton, FL, USA, 2018; Volume 2.
36. Drzymala, J.; Kowalczyk, P.B. Classification of Flotation Frothers. *Minerals* **2018**, *8*, 53. [[CrossRef](#)]
37. Bhatia, S.P.; Letizia, C.S.; Api, A.M. Fragrance material review on alpha-terpineol. *Food Chem. Toxicol.* **2008**, *46*, S280–S285. [[CrossRef](#)]
38. Khaleel, C.; Tabanca, N.; Buchbauer, G. alpha-Terpineol, a natural monoterpene: A review of its biological properties. *Open Chem.* **2018**, *16*, 349–361. [[CrossRef](#)]
39. Chang, C.H.; Franses, E.I. Dynamic Tension Behavior of Aqueous Octanol Solutions under Constant-Area and Pulsating-Area Conditions. *Chem. Eng. Sci.* **1994**, *49*, 313–325. [[CrossRef](#)]
40. Zawala, J.; Wiertel-Pochopien, A.; Kowalczyk, P.B. Critical Synergistic Concentration of Binary Surfactant Mixtures. *Minerals* **2020**, *10*, 192. [[CrossRef](#)]
41. Zawala, J.; Wiertel-Pochopien, A.; Larsen, E.; Kowalczyk, P.B. Synergism between Cationic Alkyltrimethylammonium Bromides (C(n)TAB) and Nonionic n-Octanol in the Foamability of Their Mixed Solutions. *Ind. Eng. Chem. Res.* **2020**, *59*, 1159–1167. [[CrossRef](#)]
42. Kosior, D.; Zawala, J.; Malysa, K. When and how  $\alpha$ -terpineol and n-octanol can inhibit bubble attachment to hydrophobic surfaces. *Physicochem. Probl. Mineral Pro.* **2011**, *47*, 169–182.
43. Vejrazka, J.; Fujasova, M.; Stanovsky, P.; Ruzicka, M.C.; Drahos, J. Bubbling controlled by needle movement. *Fluid Dyn. Res.* **2008**, *40*, 521–533. [[CrossRef](#)]
44. Okada, K.; Akagi, Y.; Kogure, M.; Yoshioka, N. Effect on surface-charges of bubbles and fine particles on air flotation process. *Can. J. Chem. Eng.* **1990**, *68*, 393–399. [[CrossRef](#)]
45. Uddin, S.; Jin, L.; Mirnezami, M.; Finch, J.A. An apparatus to measure electrical charge of bubble swarms. *J. Colloid Interface Sci.* **2013**, *389*, 298–305. [[CrossRef](#)]
46. Zawala, J.; Karaguzel, C.; Wiertel, A.; Sahbaz, O.; Malysa, K. Kinetics of the bubble attachment and quartz flotation in mixed solutions of cationic and non-ionic surface-active substances. *Colloid Surf. A-Physicochem. Eng. Asp.* **2017**, *523*, 118–126. [[CrossRef](#)]

- 
47. Wiertel-Pochopien, A.; Zawala, J. Influence of dynamic adsorption layer formation on bubble attachment to quartz and mica surfaces in solutions of pure and mixed surface-active substances. *Physicochem. Probl. Mineral Pro.* **2018**, *54*, 1083–1094.
  48. Chang, C.H.; Franses, E.I. Adsorption Dynamics of Surfactants at the Air/Water Interface—A Critical-Review of Mathematical-Models, Data, and Mechanisms. *Colloid Surf. A-Physicochem. Eng. Asp.* **1995**, *100*, 1–45. [[CrossRef](#)]
  49. Abi Chebel, N.; Risso, F.; Masbernat, O. Inertial modes of a periodically forced buoyant drop attached to a capillary. *Phys. Fluids* **2011**, *23*, 102104. [[CrossRef](#)]